crystals

MDPI

Article

$Bi_{0.5}Na_{0.5}TiO_3$-$Bi_{3.25}La_{0.75}Ti_3O_{12}$ Lead-Free Thin Films for Energy Storage Applications through Nanodomain Design

Wenfeng Yue [1,2], Tingting Jia [1,3,*], Yanrong Chen [1], Wenbin Dai [1], Liang Yu [1,2], Yali Cai [1,3], Ting Li [1], Lixia Liu [1], Quansheng Guo [3] and Shuhui Yu [1]

[1] Shenzhen Institute of Advanced Electronic Materials, Shenzhen Institute of Advanced Technology, Chinese Academy of Sciences, Shenzhen 518055, China
[2] Nano Science and Technology Institute, University of Science And Technology of China, Suzhou 215123, China
[3] School of Materials Science and Engineering, Hubei University, Wuhan 430062, China
* Correspondence: tt.jia@siat.ac.cn

Abstract: Dielectric capacitors have received increasing attention due to their high power density. The Bi-based Aurivillius phase compound $Bi_{3.25}La_{0.75}Ti_3O_{12}$ (BLT) is considered a potential material in the field of energy storage due to its excellent ferroelectric properties and good fatigue resistance, and temperature stability. In this paper, $0.4Bi_{0.5}Na_{0.5}TiO_3$-$0.6Bi_{3.25}La_{0.75}Ti_3O_{12}$ (0.4NBT4BNT-0.6BLT)-thin films were prepared on $Pt/Ti/SiO_2/Si$ substrates with the sol-gel method. The addition of BNT destroys the long-range ferroelectric order of BLT and forms nanodomains. By increasing the BNT content, the BLT is transformed from a ferroelectric state to a relaxed state, and its application in the field of energy storage is realized. The recoverable energy density is 42.41 J/cm^3, and the recoverable energy storage density is relatively stable in the range of 25–200 °C with good thermal stability. The energy storage efficiency is 75.32% at ~2663 kV/cm. The leakage current density at 300 kV/cm is 1.06×10^{-9} A/cm^2.

Keywords: energy storage; nanodomain; $Bi_{3.25}La_{0.75}Ti_3O_{12}$; thin film

Citation: Yue, W.; Jia, T.; Chen, Y.; Dai, W.; Yu, L.; Cai, Y.; Li, T.; Liu, L.; Guo, Q.; Yu, S. $Bi_{0.5}Na_{0.5}TiO_3$-$Bi_{3.25}La_{0.75}Ti_3O_{12}$ Lead-Free Thin Films for Energy Storage Applications through Nanodomain Design. *Crystals* **2022**, *12*, 1524. https://doi.org/10.3390/cryst12111524

Academic Editor: Alexei A. Bokov

Received: 14 September 2022
Accepted: 22 October 2022
Published: 26 October 2022

1. Introduction

With the rapid development of the electronic industry and the trend of miniaturization and integration of integrated circuits, dielectric capacitors with high energy storage density and energy storage efficiency have attracted increasing attention [1–5]. Typically, the recoverable energy storage density (U_{rec}) and energy efficiency (ŋ) is calculated by integrating the hysteresis loop as follows [6–8]:

$$U_{rec} = \int_{P_r}^{P_{max}} EdP$$

$$ŋ = U_{rec}/(U_{rec} + U_{loss})$$

Here, E is the applied electric field, P_{max} is the maximum polarization, P_r is the remnant polarization. Therefore, materials with a large P_{max}, small P_r, and high breakdown field strength are potential candidates for high energy storage performance. Previously, commercial energy storage materials were mainly lead-based. However, the volatilization of lead in lead-based materials would not only cause harm to the human body but also pollute the environment [9–11]. Therefore, it is imperative to replace lead-based materials with lead-free materials. Lead-free thin-film materials have also achieved many exciting results. For example, Zhang et al. achieved enhanced energy storage performance in $0.9Na_{0.5}Bi_{0.5}TiO_3$-$0.1BiFeO_3$ (0.9NBT-0.1BFO) thin films prepared by adding BFO to the lead-free material system NBT, with a recoverable energy density of 44 J/cm^3 [12]; Song et al.

obtained an energy storage density of 47.6 J/cm^3 and an energy storage efficiency of 65.68% by doping 2% Mn into lead-free $0.7Sr_{0.7}Bi_{0.2}TiO_3$-$0.3BiFeO_3$ film to reduce the oxygen vacancy content of the material [13]. In order to meet the application of power devices in various fields, it is necessary to further develop lead-free dielectric capacitors with high energy storage performance.

At present, the main ways to improve the energy storage properties of materials are domain engineering [14–16], structural design [4,6,17,18], and element doping [13,19–21]. In general, slender hysteretic loops with low energy dissipation can be achieved by customizing the ferroelectric (FE) or anti-ferroelectric (AFE) domain sizes to the micron or nanoscale. Due to a local random field, the relaxation ferroelectric (RFE) with a polar nanoregion requires a very high applied electric field to construct a saturated long-range order, resulting in enhanced energy storage densities. Song et al. reported that the long-range order of anti-ferroelectric domains could be destroyed by introducing lanthanum (La) into $AgNbO_3$ ceramics. Thus, the micron-level anti-ferroelectric domains were transformed into anti-ferroelectric nanodomains, resulting in a lower residual polarization, larger breakdown electric field strength, and higher energy density and efficiency [22]. By adding $SrTiO_3$(STO) into $BiFeO_3$(BFO), Pan et al. transformed its ferroelectric microdomains into nanodomains with high dynamic polarity, from ferroelectric to relaxor ferroelectric and obtained a high energy storage density and efficiency through domain engineering [23]. All the results show that domain engineering effectively improves the dielectric capacitor's storage characteristics. However, these energy storage materials can only maintain good energy storage performance at low temperatures (<120 °C), so it is necessary to explore a kind of energy storage material that can achieve good energy storage performance through domain engineering and make it work stably at a high temperature.

$Bi_4Ti_3O_{12}$ (BIT) belongs to the Aurivillius family of oxides. It consists of a $(Bi_2O_2)^{2+}$ layer and a perovskite $(A_{n-1}B_nO_{3n+1})^{2-}$ layer, which has excellent fatigue resistance and temperature stability, and its improved ferroelectric properties can be found in the study of its A-site doping La, which has broad application prospects in non-volatile ferroelectric memories [24–27]. In addition, its large polarization, small leakage current density, excellent anti-fatigue properties, and temperature stability determine its application in the field of energy storage [28]. However, its large residual polarization and low breakdown strength limit its application in the field of energy storage. Therefore, it is necessary to reduce its residual polarization and improve its breakdown field strength.

In this work, we selected another Bi-based material with a higher Curie temperature (Tc = 320 °C)-$Bi_{0.5}Na_{0.5}TiO_3$(BNT), to be incorporated into the BLT. It causes compositional and chemical disorder in 0.4BNT-0.6BLT films, which breaks the long-range FE order of BLT. With the addition of BNT, the long-range ferroelectric order of BLT is destroyed, resulting in nanodomains. The RFE state induced by domain engineering achieves suppressed residual polarization and enhanced breakdown strength, and maintains a large polarization value of BNT. Excellent energy storage performance, a small leakage current density, and good temperature stability (25–200 °C) are obtained in 0.4BNT-0.6BLT thin films.

2. Experiments

$0.4Bi_{0.5}Na_{0.5}TiO_3$-$0.6Bi_{3.25}La_{0.75}Ti_3O_{12}$ (0.4BNT-0.6BLT) thin films were grown on $Pt/Ti/SiO_2/Si$ substrates with the sol-gel method. The precursor solution uses bismuth(III) acetate, lanthanum acetate, sodium acetate, and tetrabutyl titanate as raw materials, propionic acid as a solvent, and ethanolamine as a stabilizer. Bismuth acetate, lanthanum acetate, sodium acetate, and tetrabutyl titanate were weighed according to the stoichiometric ratio. To compensate for the volatilization of bismuth and sodium during annealing, a 5% excess of bismuth acetate and sodium acetate was used to prepare the precursor solution. First, bismuth acetate, sodium acetate, and lanthanum acetate were added to propionic acid in turn, and stirred at room temperature until fully dissolved. Tetrabutyl titanate was added, and a certain amount of ethanolamine was added to stabilize the colloid and stirred at room temperature for one day to obtain a golden yellow precursor solution. The solution

was spun at 6000 rpm for 20 s and then pyrolyzed on a hot stage at 400 °C for 6 min; this process was repeated a certain number of times to obtain thin film samples with a certain thickness. Finally, the samples were rapidly annealed in an air atmosphere in an infrared annealing furnace at 700 °C. The same process was used to prepare the BLT film.

The crystallinity and phase of the samples were characterized by performing X-ray diffraction (XRD), the elemental distribution of the sample was tested with an energy dispersive spectroscopy (EDS), and the domain structure of the samples was characterized by piezoelectric atomic force microscopy (PFM). The ferroelectric properties of the samples were investigated using a ferroelectric tester (Radiant Technology, Albuquerque, NM, USA) before electrical testing. Au top electrodes with a diameter of 0.5 mm were deposited on the films by magnetron sputtering through a reticle to obtain Au/BNT-BLT/Pt capacitors.

3. Results and Discussion

The XRD patterns of 0.4BNT-0.6BLT films grown on Pt/Ti/SiO_2/Si substrates with the sol-gel method are shown in Figure 1. Compared with the (117) preferred orientation of pure BLT films, 0.4BNT-0.6BLT showed no obvious preference orientation. Moreover, all the characteristic peaks of BNT-BLT were assigned to the $Bi_4Ti_3O_{12}$ phase. Energy dispersive spectroscopy confirmed the formation of a homogeneous NBT-BLT solid solution. As shown in Figure 1b, bismuth, lanthanum, titanium, and sodium elements were uniformly dispersed in the film without apparent aggregation.

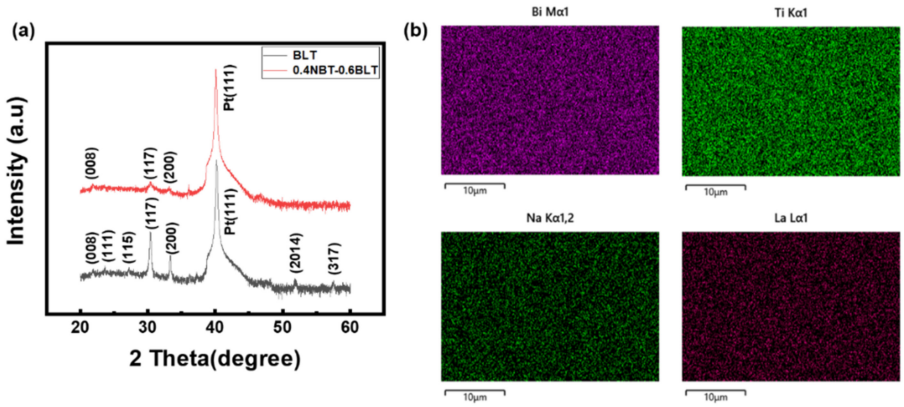

Figure 1. (**a**) XRD patterns of BLT and BNT-BLT. (**b**) EDS spectrum of BNT-BLT.

The typical morphology (AFM) images of the 0.4BNT-0.6BLT films are shown in Figure 2. All films exhibit good surface density and roughness. The root-mean-square (RMS) of surface roughness of the BLT film was calculated with Igor Pro software, and was found to be 7.62; the RMS value of the 0.4BNT-0.6BLT film is 5.29 nm, which indicates that all the films show a very smooth surface. The suitable microstructure and surface morphology indicate that the electrical properties of the films improved, including a reduced leakage current and tolerable electric field strength, which are discussed in the next section.

Figure 3 shows the phase image of the random region of the BNT-BLT thin film. Regions with bright contrast are polarized in opposite directions to regions with dark contrast, where bright and dark regions represent upper and lower polarizations, respectively. Figure 3a shows the phase map zoomed in at random regions, and a linear domain structure with a width of nanometers is found. Figure 3b shows the phase in the region corresponding to the red line in Figure 3a [29], indicating that in the BNT-BLT thin film material system, the addition of BNT can disrupt the long-range ferroelectric order state in the BLT matrix, reducing the macrodomain size and the transformation to the nanodomain structure.

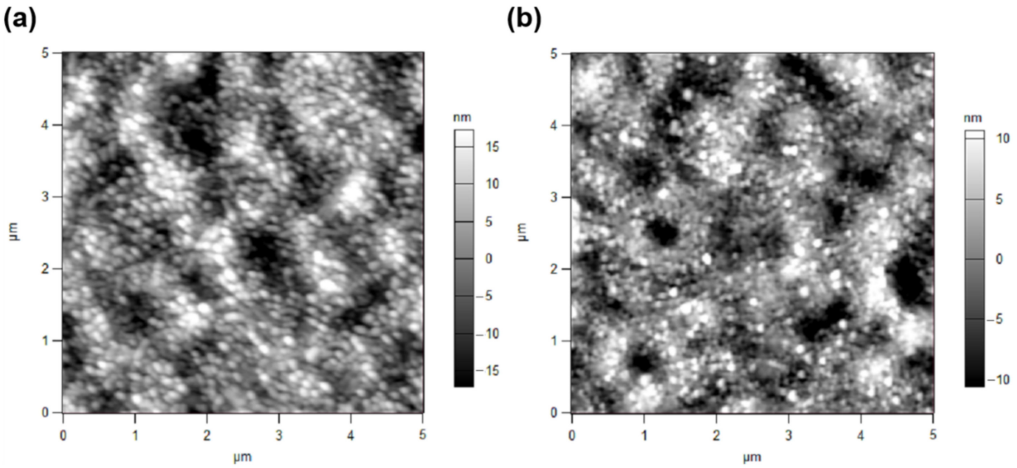

Figure 2. The surface micrographs of all thin films (**a**) BLT, (**b**) 0.4BNT0.6BLT.

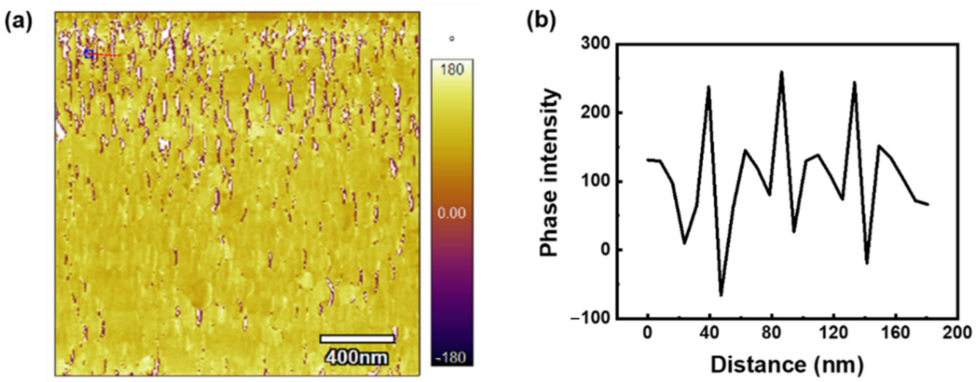

Figure 3. PFM images of 0.4BNT-0.6BLT; (**a**) Phase image of 0.4BNT-0.6BLT with 2 × 2 μm^2 scanning area; (**b**) the phase diagram of the cross-section in (**a**).

Figure 4a,b show the hysteresis loops of the BNT-BLT films under different electric fields. It can be found that the BLT films exhibit typical ferroelectricity, while the BNT-BLT films exhibit relaxed ferroelectricity. This is because the addition of BNT disrupts the long-range ferroelectric order of BLT, inducing a nanoscale domain structure and polar nanoscale regions (PNRs). The appearance of nanodomains and PNRs leads to a decrease in remnant polarization and thinner P-E rings. The reduction in domain size can enhance the relaxation behavior of ferroelectrics, in which more dipoles return to the disordered state when the applied field is removed. Therefore, the remanent polarization of BNT-BLT is maintained at a low level. Figure 4c shows the P_{max} and P_r of BNT-BLT as a function of the electric field, respectively. As the electric field increases, P_{max} and P_r increase at different growth rates, and ΔP also increases in this case ($\Delta P = P_{max} - P_r$), which is beneficial for energy storage. A higher breakdown strength is also necessary for energy storage. BNT-BLT exhibits good breakdown strength, and the maximum breakdown voltage can reach ~2663 kV/cm, which is related to its smaller leakage current shown in Figure 5. According to the hysteresis loop, the energy storage characteristics of BNT-BLT are calculated. As shown in Figure 4d, when 0.4BNT-0.6BLT is at 2662.675 kV/cm, the recoverable energy density is 42.41 J/cm^3, and the energy efficiency is 75.32%.

The leakage current density and electric field (J-E) characteristics of BLT and 0.4BNT-0.6BLT films are shown in Figure 5. Compared with the BLT film, the leakage current of the 0.4BNT-0.6BLT film is significantly reduced. Its leakage current density at 300 kV/cm is 1.06 × 10^{-9} A/cm^2 and for BLT it is about 10^{-8} A/cm^2. It may be due to the increase in the number of grain boundaries, which is due to the decrease in grain size. The increased grain boundaries hinder the onset of defect diffusion and also contribute to reducing the current density [30].

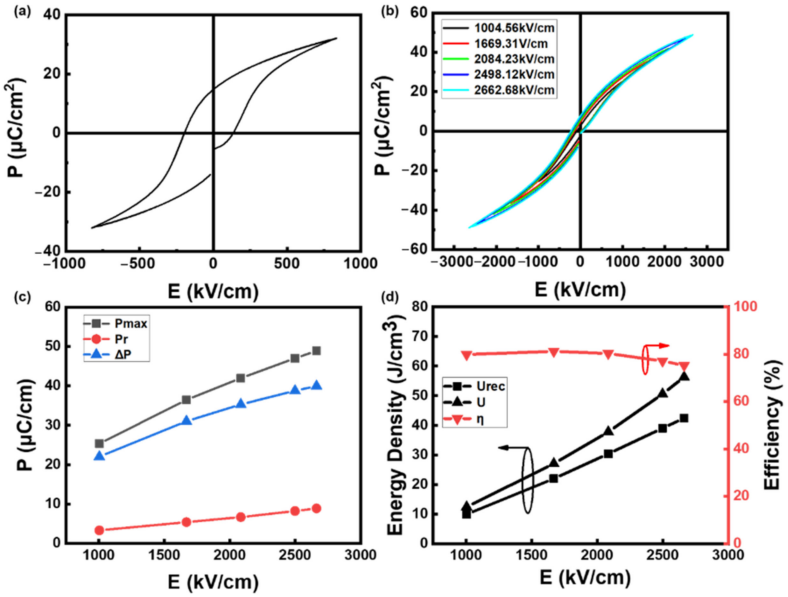

Figure 4. Hysteresis loop of (**a**) BLT, (**b**) 0.4BNT-0.6BLT; variation of (**c**) polarization and (**d**) energy storage properties with electric field strength for 0.4BNT0.6BLT at 10 kHz.

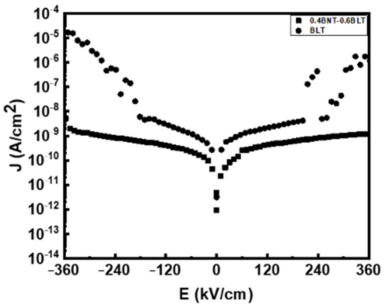

Figure 5. Leakage current density vs. electric field (JE) curves of BLT and 0.4BNT0.6BLT films.

Figure 6a shows the hysteresis loops of the 0.4BNT-0.6BLT film measured from 25 to 200 °C under an applied electric field of 1500 kV/cm. A typical P-E curve is obtained. Figure 6b shows the variation of P_{max} and P_r with the electric field at different temperatures. When the temperature is below 100 °C, P_{max} decreases slightly. When it is above 100 °C, P_{max} begins to increase greatly, while P_r increases with temperature. This is because domain wall motion is easier when the temperature increases. However, the obvious increase in P_r is slightly larger than P_{max}, resulting in the decrease in ΔP, which is not good for the energy storage performance. When the temperature increased from 25 to 200 °C, U_{rec} decreased from 18.10 to 17.08 J/cm^3, the change of U_{rec} was only 5.65%, and ŋ decreased from 84.25 to 76.64%, indicating that 0.4BNT-0.6BLT has good thermal stability.

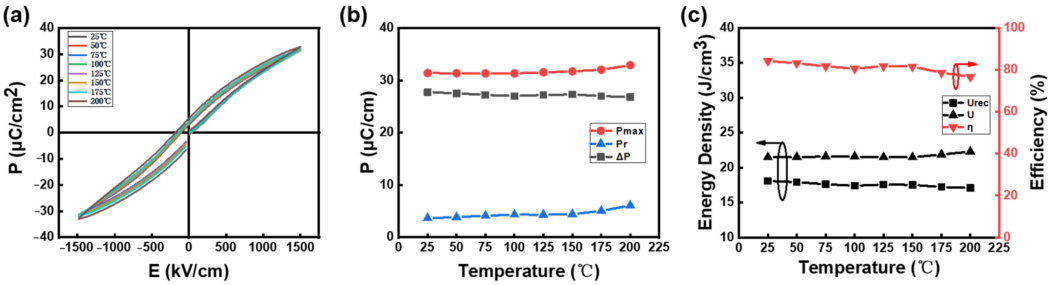

Figure 6. (**a**) Hysteresis loop, (**b**) polarization and (**c**) energy storage characteristics as a function of temperature, at 1500 kV/cm, 10 kHz.

4. Conclusions

In summary, BLT and 0.4BNT-0.6BLT thin films were prepared on $Pt/Ti/SiO_2/Si$ substrates using the sol-gel method. The introduction of BNT destroys the long-range order of the BLT ferroelectric domain structure, leading to the transitions from microdomains to nanodomains. A lower remnant polarization and a larger remnant polarization were obtained, a recoverable energy density of 42.41 J/cm^3 was obtained at ~2663 kV/cm, the energy storage efficiency was 75.32%, and the leakage current density at 300 kV/cm was 1.06×10^{-9} A/cm^2. There is no obvious change in the recoverable energy storage density in the range of 25–200 °C, which indicates that it has good thermal stability. These properties indicate that the lead-free material 0.4BNT-0.6BLT has a good application prospect in the field of energy storage. This work provides a reference for preparing dielectric energy storage materials with excellent energy storage properties by domain engineering.

Author Contributions: Conceptualization, W.Y. and T.J.; methodology, W.Y., Y.C. (Yanrong Chen) and W.D.; software, W.Y.; validation, L.Y. and Y.C. (Yali Cai); formal analysis, W.Y. and T.L.; investigation, W.Y. and L.L.; resources, T.J. and S.Y.; data curation, W.Y.; writing—original draft preparation, W.Y.; writing—review and editing, T.J. and Q.G.; visualization, T.L.; supervision, T.J.; project administration, T.J.; funding acquisition, T.J. and S.Y. All authors have read and agreed to the published version of the manuscript.

Funding: This research was funded by the National Natural Science Foundation of China (51702351, 51777209), the Basic and Applied Basic Research Foundation of Guangdong Province (2020B1515120019), and the Shenzhen Science and Technology Innovation Committee (JCYJ20170413152832151, KQTD20170810160424889).

Data Availability Statement: This date that support the finding of this study are available from the corresponding author upon reasonable request.

Conflicts of Interest: The authors declare no conflict of interest.

References

1. Pan, H.; Li, F.; Liu, Y.; Zhang, Q.; Wang, M.; Lan, S.; Zheng, Y.; Ma, J.; Gu, L.; Shen, Y.; et al. Ultrahigh–energy density lead-free dielectric films via polymorphic nanodomain design. *Science* **2019**, *365*, 578–582. [CrossRef] [PubMed]
2. Pan, H.; Lan, S.; Xu, S.; Zhang, Q.; Yao, H.; Liu, Y.; Meng, F.; Guo, E.-J.; Gu, L.; Yi, D.; et al. Ultrahigh energy storage in superparaelectric relaxor ferroelectrics. *Science* **2021**, *374*, 100–104. [CrossRef] [PubMed]
3. Silva, J.P.B.; Sekhar, K.C.; Pan, H.; MacManus-Driscoll, J.L.; Pereira, M. Advances in Dielectric Thin Films for Energy Storage Applications, Revealing the Promise of Group IV Binary Oxides. *ACS Energy Lett.* **2021**, *6*, 2208–2217. [CrossRef]
4. Zhu, H.; Liu, M.; Zhang, Y.; Yu, Z.; Ouyang, J.; Pan, W. Increasing energy storage capabilities of space-charge dominated ferroelectric thin films using interlayer coupling. *Acta Mater.* **2017**, *122*, 252–258. [CrossRef]
5. Yang, L.; Kong, X.; Li, F.; Hao, H.; Cheng, Z.; Liu, H.; Li, J.-F.; Zhang, S. Perovskite lead-free dielectrics for energy storage applications. *Prog. Mater. Sci.* **2019**, *102*, 72–108. [CrossRef]
6. Mao, N.; Meng, L.; Li, Y.; Hu, Z.; Chu, J. Enhanced voltage endurance capability of Ba(Zr0.2Ti0.8)O3 thin films induced by atomic-layer-deposited Al2O3 intercalations and the application in electrostatic energy storage. *Ceram. Int.* **2021**, *47*, 7720–7727. [CrossRef]
7. Ding, J.; Pan, Z.; Chen, P.; Hu, D.; Yang, F.; Li, P.; Liu, J.; Zhai, J. Enhanced energy storage capability of (1-x)Na0.5Bi0.5TiO3-xSr0.7Bi0.2TiO3 free-lead relaxor ferroelectric thin films. *Ceram. Int.* **2020**, *46*, 14816–14821. [CrossRef]
8. Nguyen, M.D. Impact of fatigue behavior on energy storage performance in dielectric thin-film capacitors. *J. Eur. Ceram. Soc.* **2020**, *40*, 1886–1895. [CrossRef]
9. Nguyen, M.D.; Nguyen, C.T.Q.; Vu, H.N.; Rijnders, G. Controlling microstructure and film growth of relaxor-ferroelectric thin films for high break-down strength and energy-storage performance. *J. Eur. Ceram. Soc.* **2018**, *38*, 95–103. [CrossRef]
10. Ahn, C.W.; Amarsanaa, G.; Won, S.S.; Chae, S.A.; Lee, D.S.; Kim, I.W. Antiferroelectric Thin-Film Capacitors with High Energy-Storage Densities, Low Energy Losses, and Fast Discharge Times. *ACS Appl. Mater. Interfaces* **2015**, *7*, 26381–26386. [CrossRef]
11. Ma, B.; Hu, Z.; Koritala, R.E.; Lee, T.H.; Dorris, S.E.; Balachandran, U. PLZT film capacitors for power electronics and energy storage applications. *J. Mater. Sci. Mater. Electron.* **2015**, *26*, 9279–9287. [CrossRef]
12. Zhang, J.; Song, J.; Li, X.; Dong, G.; Zhao, L. Enhanced energy storage performance in 0.9NBT-0.1BFO thin film. *Mater. Lett.* **2020**, *276*, 128266. [CrossRef]
13. Song, B.; Wu, S.; Yan, H.; Zhu, K.; Xu, L.; Shen, B.; Zhai, J. Fatigue-less relaxor ferroelectric thin films with high energy storage density via defect engineer. *J. Mater. Sci. Technol.* **2021**, *77*, 178–186. [CrossRef]

14. Qi, H.; Xie, A.; Tian, A.; Zuo, R. Superior Energy-Storage Capacitors with Simultaneously Giant Energy Density and Efficiency Using Nanodomain Engineered $BiFeO_3$-$BaTiO_3$-$NaNbO_3$ Lead-Free Bulk Ferroelectrics. *Adv. Energy Mater.* **2019**, *10*, 1903338. [CrossRef]
15. Qi, H.; Zuo, R.; Xie, A.; Tian, A.; Fu, J.; Zhang, Y.; Zhang, S. Ultrahigh Energy-Storage Density in $NaNbO_3$-Based Lead-Free Relaxor Antiferroelectric Ceramics with Nanoscale Domains. *Adv. Funct. Mater.* **2019**, *29*, 1903877. [CrossRef]
16. Xie, A.; Qi, H.; Zuo, R.; Tian, A.; Chen, J.; Zhang, S. An environmentally-benign $NaNbO_3$ based perovskite antiferroelectric alternative to traditional lead-based counterparts. *J. Mater. Chem. C* **2019**, *7*, 15153–15161. [CrossRef]
17. Spahr, H.; Nowak, C.; Hirschberg, F.; Reinker, J.; Kowalsky, W.; Hente, D.; Johannes, H.H. Enhancement of the maximum energy density in atomic layer deposited oxide based thin film capacitors. *Appl. Phys. Lett.* **2013**, *103*, 042907. [CrossRef]
18. Sun, Z.; Ma, C.; Liu, M.; Cui, J.; Lu, L.; Lu, J.; Lou, X.; Jin, L.; Wang, H.; Jia, C.L. Ultrahigh Energy Storage Performance of Lead-Free Oxide Multilayer Film Capacitors via Interface Engineering. *Adv. Mater.* **2017**, *29*, 1604427. [CrossRef]
19. Li, Q.; Ji, S.; Wang, D.; Zhu, J.; Li, L.; Wang, W.; Zeng, M.; Hou, Z.; Gao, X.; Lu, X.; et al. Simultaneously enhanced energy storage density and efficiency in novel $BiFeO_3$-based lead-free ceramic capacitors. *J. Eur. Ceram. Soc.* **2021**, *41*, 387–393. [CrossRef]
20. Song, D.P.; Yang, J.; Yang, B.B.; Wang, Y.; Chen, L.Y.; Wang, F.; Zhu, X.B. Energy storage in $BaBi_4Ti_4O_{15}$ thin films with high efficiency. *J. Appl. Phys.* **2019**, *125*, 134101. [CrossRef]
21. Nguyen, M.D. Ultrahigh energy-storage performance in lead-free BZT thin-films by tuning relaxor behavior. *Mater. Res. Bull.* **2021**, *133*, 111072. [CrossRef]
22. Li, S.; Hu, T.; Nie, H.; Fu, Z.; Xu, C.; Xu, F.; Wang, G.; Dong, X. Giant energy density and high efficiency achieved in silver niobate-based lead-free antiferroelectric ceramic capacitors via domain engineering. *Energy Storage Mater.* **2021**, *34*, 417–426. [CrossRef]
23. Pan, H.; Ma, J.; Ma, J.; Zhang, Q.; Liu, X.; Guan, B.; Gu, L.; Zhang, X.; Zhang, Y.J.; Li, L.; et al. Giant energy density and high efficiency achieved in bismuth ferrite-based film capacitors via domain engineering. *Nat. Commun.* **2018**, *9*, 1813. [CrossRef] [PubMed]
24. Park, B.H.; Kang, B.S.; Bu, S.D.; Noh, T.W.; Lee, J.; Jo, W. Lanthanum-substituted bismuth titanate for use in non-volatile memories. *Nature* **1999**, *401*, 682–684. [CrossRef]
25. Subbarao, E.C. A family of ferroelectric bismuth compounds. *J. Phys. Chem. Solids* **1962**, *23*, 665–676. [CrossRef]
26. Long, C.; Chang, Q.; Fan, H. Differences in nature of electrical conductions among $Bi_4Ti_3O_{12}$-based ferroelectric polycrystalline ceramics. *Sci. Rep.* **2017**, *7*, 4193. [CrossRef]
27. Chen, Y.; Xie, S.; Wang, H.; Chen, Q.; Wang, Q.; Zhu, J.; Guan, Z. Dielectric abnormality and ferroelectric asymmetry in W/Cr co-doped $Bi_4Ti_3O_{12}$ ceramics based on the effect of defect dipoles. *J. Alloys Compd.* **2017**, *696*, 746–753. [CrossRef]
28. Sun, J.; Han, Y.; Gao, G.; Yang, J.; Zhang, Y.; Dai, Y.; Song, D. Breakdown field enhancement and energy storage performance in four-layered Aurivillius films. *Ceram. Int.* **2022**, *48*, 15780–15784. [CrossRef]
29. Chang, W.-Y.; Chung, C.-C.; Yuan, Z.; Chang, C.-H.; Tian, J.; Viehland, D.; Li, J.-F.; Jones, J.L.; Jiang, X. Patterned nano-domains in PMN-PT single crystals. *Acta Mater.* **2018**, *143*, 166–173. [CrossRef]
30. Pan, Z.; Wang, P.; Hou, X.; Yao, L.; Zhang, G.; Wang, J.; Liu, J.; Shen, M.; Zhang, Y.; Jiang, S.; et al. Fatigue-Free Aurivillius Phase Ferroelectric Thin Films with Ultrahigh Energy Storage Performance. *Adv. Energy Mater.* **2020**, *10*, 2001536. [CrossRef]